The Twisted Configuration of the Martian Magnetotail: MAVEN Observations

Gina A. DiBraccio[1], Janet G. Luhmann[2], Shannon M. Curry[2], Jared R. Espley[1], Shaosui Xu[2], David L. Mitchell[2], Yingjuan Ma[3], Chuanfei Dong[4], Jacob R. Gruesbeck[1,5], John E.P. Connerney[1,6], Yuki Harada[7], Suranga Ruhunusiri[7], Jasper S. Halekas[7], Yasir Soobiah[1,5], Takuya Hara[2], David A. Brain[8], and Bruce M. Jakosky[8]

[1]Solar System Exploration Division, NASA Goddard Space Flight Center, Greenbelt, Maryland, USA.

[2]Space Sciences Laboratory, University of California, Berkeley, California, USA.

[3]Department of Earth, Planetary and Space Sciences, UCLA, Los Angeles, California, USA.

[4]Department of Astrophysical Sciences and Princeton Plasma Physics Laboratory, Princeton University, Princeton, New Jersey, USA.

[5]Department of Astronomy, University of Maryland, College Park, Maryland, USA.

[6]Space Research Corporation, Annapolis, Maryland, USA.

[7]Department of Physics and Astronomy, The University of Iowa, Iowa City, Iowa, USA.

[8]Laboratory for Atmospheric and Space Physics, University of Colorado, Boulder, Colorado, USA.

Corresponding author: G. A. DiBraccio, Solar System Exploration Division, NASA Goddard Space Flight Center, Greenbelt, MD 20771, USA. (gina.a.dibraccio@nasa.gov)

This article has been accepted for publication and undergone full peer review but has not been through the copyediting, typesetting, pagination and proofreading process which may lead to differences between this version and the Version of Record. Please cite this article as doi: 10.1029/2018GL077251

Key points

- MAVEN data and simulations confirm a twisted field configuration is present in the Martian magnetotail that is highly dependent on IMF B_Y
- Open fields, likely created by magnetic reconnection between Mars crustal fields and the IMF, occupy a majority of the twisted tail lobes
- Comparisons with Earth suggest the dipolar component of Mars' crustal fields play a crucial role in altering the magnetotail structure

Abstract

Measurements provided by the Mars Atmosphere and Volatile EvolutioN (MAVEN) spacecraft are analyzed to investigate the Martian magnetotail configuration as a function of IMF B_Y. We find that the magnetotail lobes exhibit a ~45° twist, either clockwise or counterclockwise from the ecliptic plane, up to a few Mars radii downstream. Moreover, the associated cross-tail current sheet is rotated away from the expected location for a Venus-like induced magnetotail based on nominal interplanetary magnetic field (IMF) draping. Data-model comparisons using magnetohydrodynamic simulations are in good agreement with the observed tail twist. Model field line tracings indicate that a majority of the twisted tail lobes are composed of open field lines, surrounded by draped IMF. We infer that dayside magnetic reconnection between the crustal fields and draped IMF creates these open fields and may be responsible for the twisted tail configuration, similar to what is observed at Earth.

This study investigates the magnetic environment of Mars in order to understand how its structure is different from other planets. In the past, it was thought that the Sun's magnetic field interacts with Mars in a similar way to that of a comet or Venus. This would imply that the magnetic field geometry could be easily predicted; however, recent investigations have found that this is not the case. This work includes both simulation and MAVEN data to determine that the magnetic environment of Mars is much different than this original picture. The conclusions find that these fields are twisted from their expected geometry, suggesting a difference in the interaction between Mars and the Sun. Because atmospheric particles are able to travel along these magnetic fields, this unique geometry may have great implications for atmospheric loss at Mars.

1. Introduction

The Martian magnetosphere is a complex magnetic environment, unlike any other in our solar system. To first order, this magnetosphere forms as the upstream interplanetary magnetic field (IMF) drapes around the planet while interacting with the obstacle presented by the upper atmosphere and ionosphere [*Nagy et al.*, 2004]. Early Mars missions that carried magnetometers revealed that this interaction results in a dual-lobe magnetotail with a central cross-tail current sheet, similar to a comet- or Venus-like interaction with the solar wind [*Yeroshenko et al.*, 1990; *Luhmann et al.*, 1991; *Fedorov et al.*, 2006; *Bertucci et al.*, 2011]. At Mars, however, this induced magnetosphere paradigm is complicated by the presence of the localized crustal magnetic fields [*Acuna et al.*, 1998; 1999].

The strongest crustal sources are located near 180°E longitude [*Connerney et al.*, 2001] and rotate with the planet, creating an ever-changing obstacle to the upstream solar wind. Furthermore, these planetary fields are able to undergo magnetic reconnection with the impinging IMF [*Brain*, 2006; *Halekas et al.*, 2009; *Harada et al., Magnetic reconnection on*

dayside crustal magnetic fields at Mars: MAVEN observations, submitted to Geophys. Res. Lett., 2018]. This occurrence of reconnection introduces new field topologies and electric currents throughout the system. In particular, the structure of the Martian magnetotail is populated with a variety of field topologies [*Brain et al.*, 2007; *Weber et al.*, 2017; *Xu et al.*, 2017a; *Xu et al.*, 2017b] that facilitate the transport of mass, energy, and momentum through an assortment of processes. At Mars, observations of magnetic reconnection [*Dubinin et al.*, 2008; *Eastwood et al.*, 2008; *Harada et al.*, 2015a; 2017], flux rope formation [*Eastwood et al.*, 2012; *DiBraccio et al.*, 2015; *Hara et al.*, 2017], current sheet flapping [*DiBraccio et al.*, 2017], Marsward and tailward ion flows [*Harada et al.*, 2015b], magnetic lobe dependence on IMF orientation [*Crider et al.*, 2004; *Romanelli et al.*, 2015] and ionosphere magnetization [*Liemohn et al.*, 2017], and bulk plasma escape [e.g., *Brain et al.*, 2010; *Halekas et al.*, 2016] have been reported in the magnetotail. These dynamics have direct magnetospheric consequences, including both energy deposition into the upper atmosphere and tailward particle acceleration, which in turn, is a main contributor to atmospheric escape to space [e.g., *Dubinin et al.*, 1993; 2011; *Lundin*, 2011; *Brain et al.*, 2015; *Y Dong et al.*, 2015; 2017].

Recently, *Luhmann et al.* [2015a] described details of the magnetotail field topology from a magnetohydrodynamic (MHD) simulation of the Mars-solar wind interaction. The results suggest that a large fraction of the magnetotail lobes in the near-Mars tail may be composed of open magnetic fields, with one end connected to the planet, rather than predominantly draped IMF. Furthermore, *Luhmann et al.* [2015a] concluded that, because large portions of the Martian tail may contain fields connected to the planet, the structure does not strictly maintain an induced tail polarity pattern predicted by standard IMF draping. This shifts the paradigm of the solar wind interaction away from comet-like to a situation unique to Mars; however, *in situ* observations of the Martian tail are necessary to confirm this conceptual revision.

Now, using data from the Mars Atmosphere and Volatile EvolutioN (MAVEN) mission [*Jakosky et al.*, 2015], it is possible to observationally address this Martian magnetotail paradigm shift. MAVEN's orbit (described further in Section 2) precesses about the planet to provide global coverage of the magnetotail out to nearly three planetary radii, enabling a statistical assessment of the magnetic field configuration. Through data-model comparisons using multi-species, single fluid MHD simulations, we characterize a twisted tail configuration and assess possible field topologies responsible for the unique structure of the Martian magnetotail.

2. Analysis Tools and Methodology

This study utilizes the statistics of MAVEN *in situ* measurements and MHD simulations to enhance the scientific return of single-point spacecraft measurements. Here, MAVEN data and simulation results are reported in Mars solar orbital (MSO) coordinates: X_{MSO} is directed from the center of the planet to the center of the Sun, Z_{MSO} is perpendicular to the planet's orbital plane, and Y_{MSO} completes the right-handed system.

2.1 MAVEN Overview

The MAVEN spacecraft orbits Mars over a ~4.5-h period with periapsis and apoapsis altitudes of ~150 km and ~6200 km, respectively [*Jakosky et al.*, 2015]. An orbital inclination of 75° enables precession through latitudes and local times, providing sufficient coverage of the Martian space environment to construct global maps of average conditions at altitudes interior to apoapsis. It is important to note that, due to this precession, there are periods when MAVEN's orbit does not pass through certain regions of the local space environment. To characterize the magnetic configuration of the Martian magnetotail, we require that MAVEN measured both the upstream IMF and the magnetotail over a given orbit.

MAVEN's Magnetometer (MAG) [*Connerney et al.*, 2015] provides vector magnetic field measurements at a maximum sampling rate of 32 vectors s^{-1}. MAG data are analyzed to determine the magnetic field orientation and strength in the upstream solar wind and in the magnetotail. In this work, the magnetotail fields are analyzed using 30-s-average MAG data that has been calculated from the full resolution measurements. This 30 s resolution is more than sufficient to identify global trends in the Martian magnetosphere.

The Solar Wind Ion Analyzer (SWIA) [*Halekas et al.*, 2015] provides measurements of ion distributions at cadences up to 4 s. SWIA and MAG observations are utilized together to characterize solar wind parameters upstream of the bow shock. Periods of pristine solar wind were selected by implementing the algorithm developed by *Halekas et al.* [2017], based on measurements of bulk flow speed, proton scalar temperature, spacecraft altitude, and normalized magnetic field fluctuation levels. Specifically, the bulk flow speed is required to be greater than 200 km s^{-1} and the normalized root-sum-squared value of the magnetic field fluctuations must be less than 0.15. Therefore, this algorithm selects orbits with stable upstream IMF by omitting those with enhanced foreshock turbulence to provide a conservative selection of MAVEN orbits for use in this study. Upstream averages of proton density, temperature, and velocity, along with magnetic field strength and orientation are calculated for each selected orbit. In this study, the primary function of the *Halekas et al.* [2017] algorithm is to implement a robust, consistent method for determining the upstream IMF orientation to compare with the Martian magnetotail configuration. Therefore, this analysis excludes any orbits that did not meet the algorithm selection criteria.

2.2 Model Background

We utilize the 3-D multi-species, single fluid Block Adaptive Tree Solar-wind Roe Upwind Scheme (BATS-R-US) MHD code coupled with the 3-D Mars Thermospheric General Circulation Model (MTGCM) to simulate the Mars-solar wind interaction [*Ma et al.*, 2004; *C F Dong et al.*, 2015]. To accurately represent the Martian magnetosphere, crustal magnetic fields are included by implementing the *Arkani-Hamed* [2002] spherical harmonic model in near-Mars space, starting from an inner boundary of ~100 km altitude. The occurrence of magnetic reconnection is controlled by numerical diffusion throughout the simulation.

The MHD simulations were performed using a Mars Equinox season and typical EUV fluxes for solar maximum. The solar wind inputs represent average upstream conditions at Mars: solar wind velocity of 400 km s^{-1}, solar wind density of 4 cm^{-3}, IMF magnitude of 3 nT, and a Parker spiral angle of 56°. In order to investigate the influence of IMF orientation on magnetotail configuration, simulations were performed using both $+B_Y$, $-B_X$ and $-B_Y$, $+B_X$ IMF orientations, representing the Eastward and Westward Parker Spiral cases, respectively. Note that B_Y is, on average, the dominant IMF component at Mars' orbit. The simulations were repeated for four planetary orientations with the strongest crustal fields at noon, midnight, dawn, and dusk locations in local time.

Following these model runs, two model 'data' products were produced. In one set, we 'fly' through the simulation space along the MAVEN orbital segments used in the statistical data set and extract the average model vector fields. In the second model data product, field line tracings were performed to determine field topology by interpolating over the model vector fields within a spherical grid sample. Field lines were traced both inward to the ~100 km simulation boundary and outward to 3 R_M (where R_M is the radius of Mars, or ~3397 km).

This simulation domain covers the extent of MAVEN's orbit (see Figure 1) and enables consistent data-model comparisons. By performing these field line tracings, three topologies are defined: 1) closed field lines, with both ends connected to the lower boundary; 2) open field lines, with one end connected to the lower boundary and the other end passing through the 3 R_M sampling grid outer boundary; and 3) draped field lines, with both end passing through the outer boundary.

2.3 Statistics

To gather statistics on the Martian magnetotail configuration, we analyze all MAVEN MAG and SWIA data available from November 2014 through January 2017. For selection, we require that 1) MAVEN observed both the upstream solar wind and the magnetotail ($X_{MSO} \leq -1\ R_M$) over the course of a single orbit and 2) upstream parameters met the criteria of the *Halekas et al.* [2017] algorithm. Using these requirements, 1423 orbits were included in the analysis presented here. The MAVEN magnetotail orbital coverage based on this selection is depicted in Figure 1. A majority of the available tail measurements meeting these criteria are located within -1 $R_M \leq Y_{MSO} \leq +1\ R_M$ (Figure 1a) and -2 $R_M \leq X_{MSO} \leq -1\ R_M$ (Figures 1b and 1c).

Analysis of the observed IMF parameters for all orbits included in this study represent typical quantities at Mars' location in the inner solar system (Figures 1d-1f). The observed IMF magnitude (Figure 1d) has an average value of 3.3 nT. The IMF clock angle (Figure 1e), defined as the angle of the field vector in the Y_{MSO}-Z_{MSO} plane where 0° is along +Z_{MSO}, exhibits a bimodal distribution with average peaks at ±88°. This indicates that the IMF was mostly within the ecliptic plane, which is typical for planetary locations. The IMF Parker spiral angle (Figure 1f), defined as the angle of the field vector in the X_{MSO}-Y_{MSO} plane where

0° is along $+X_{MSO}$, demonstrates a broader bimodal distribution where the observed peaks are located at +96° and –68°.

3. Results

We investigate the effects of changing IMF direction on magnetotail configuration by examining MAG measurements of B_X in the tail (the dominant component in this region) as a function of IMF orientation. We find that the IMF B_Y played the most significant role in determining the observed patterns of occurrence of $\pm B_X$ fields and discuss these results in further detail: To analyze the tail configuration as a function of $\pm B_Y$ IMF, the orbits are first separated by IMF direction. Next, the tail B_X measurement is normalized with respect to the total field magnitude (B_X/B) and averaged over all orbits in bins of 0.1 R_M × 0.1 R_M. Cross-tail views of the average tail orientation using calculations of B_X/B are shown for $+B_Y$ and $-B_Y$ IMF in Figures 2a and 2b, respectively.

For a $+B_Y$ IMF orientation, the expected pattern of B_X in a cross-tail section would include a north-south orientation of the cross-tail current sheet with the sunward-directed tail lobe ($+B_X/B$ or red sectors in Figure 2) located in the post-midnight region ($-Y_{MSO}$) and the anti-sunward lobe ($-B_X/B$ or blue sectors in Figure 2) in the pre-midnight region ($+Y_{MSO}$). However, the observed locations of the current sheet (white on the colorbar in Figure 2) and sunward/anti-sunward lobes for $+B_Y$ IMF (Figure 2a) are twisted from this nominal configuration by ~45° in the counterclockwise direction. The $+B_X/B$ lobe is observed to encompass the northern, post-midnight tail sector while the $-B_X/B$ lobe is located in the southern, pre-midnight tail. The opposite is true for the $-B_Y$ IMF case where the current sheet and tail lobes are rotated ~45° in the clockwise direction while the $+B_X/B$ lobe is positioned in the northern, pre-midnight tail and the $-B_X/B$ lobe is located in the southern, post-midnight sector.

MAVEN observations of average tail orientation are compared with MHD simulations by implementing the same technique for normalizing and averaging B_X/B within each 0.1 R_M × 0.1 R_M bin on the extracted average model vector fields (see Section 2.2). Comparable cross-tail projections from the MHD results are presented in Figures 2c and 2d. For consistency, these model results were averaged over all four crustal field orientations because the data were not separated by crustal field location. A greater data density is required to provide an analysis based on crustal field orientation and will be performed in future work when observational statistics have increased.

The location of the modeled tail lobes and cross-tail current sheet are in agreement with the MAVEN observations. For the $+B_Y$ IMF model results in Figure 2c, the current sheet is rotated ~45° away from the north-south plane in the counterclockwise direction, causing the tail lobes to also experience this rotation. Conversely, the current sheet and tail lobes are rotated by ~45° in the clockwise direction for the $-B_Y$ IMF simulation (Figure 2d).

We find that the Martian tail configuration observed from both MAVEN data and MHD simulations are consistent and in good agreement. The current sheet orientation and magnetotail lobe positions are analogous for both the data and model projections in the $+B_Y$ (Figures 2a and 2c) and the $-B_Y$ (Figures 2b and 2d) IMF cases. From this data-model comparison we are able to confidently identify a distinct twist in the Martian magnetotail that cannot be explained simply by an induced orientation based on IMF draping.

To explore the nature of the tail twist further, we examine the closed, open, and draped field topologies determined by model field line tracings (Section 2.2). The topological conditions for the $\pm B_Y$ IMF cases with a dayside (local noon) orientation of the strong crustal fields are displayed in Figure 3 using cross-tail slices of field topologies at a downtail distance of 2 R_M. The field line tracings suggest that a majority of the Martian tail is

comprised of open field lines for both IMF scenarios at this distance. Furthermore, these open-field lobes are responsible for the observed tail twist. Within these open lobes, closed fields are observed to share this large, 45° rotation. The twisted closed- and open-field lobes are enveloped by draped fields, which do not experience the same degree of twisting. From these model results and their associated traced field footpoint locations, we infer that the open field lines were created by dayside magnetic reconnection between the closed crustal fields and draped IMF.

To examine the influence of dayside magnetic reconnection further, we present simulation results of magnetotail configuration for cases with and without the Mars crustal fields, using an upstream IMF of B_Y = +3 nT. When crustal fields are not included in the simulation (Figure 3c) the tail lobes exhibit a typical induced pattern due to draped IMF. However, when crustal fields are included with the strongest sources located at local noon (Figure 3d), the modeled tail lobes reveal a twisted configuration. This demonstrates that the presence of the Martian crustal fields, and likely their interaction with the IMF, plays a crucial role in generating the twisted tail configuration observed at Mars.

4. Discussion

For the first time, we are able to utilize global *in situ* measurements to confirm the twisted structure of the Martian magnetotail. We have performed data-model comparisons using MAVEN MAG/SWIA data along with the BATS-R-US MHD model coupled with the MTGCM and the *Arkani-Hamed* [2002] spherical harmonic crustal field model. The resulting observations and simulations are in good agreement, indicating that the magnetic configuration of the Martian tail is markedly different for periods of $+B_Y$ and $-B_Y$ IMF. The results further demonstrate that the sunward and anti-sunward lobes of the tail are twisted ~45° away from their expected location based on a purely induced tail formed by draped IMF.

Observations of this tail twist have also been recently reported in an investigation of solar wind variation effects on oxygen ion escape at Mars [*Dubinin et al.*, 2017].

By utilizing model field information including field line tracings, we have inferred that a majority of the tail is composed of open field lines, likely formed via dayside reconnection between the IMF and Martian crustal fields. An analysis of MAVEN superthermal electron data to better diagnose magnetotail field topology is also underway (see *Xu et al.* [2017a]) and will be implemented in future studies for data-model comparisons of tail field topology. The simulation results presented here suggest that dayside magnetic reconnection may be responsible for the twisted tail configuration observed at Mars. Although further work is needed to definitively support this conclusion, observations at Earth, albeit an intrinsic magnetosphere, have revealed a similar magnetotail twist with a dependence on IMF B_Y.

Cowley [1981] reported that a torque exerted by the IMF B_Y on the Earth's magnetosphere about the Sun-planet axis results in an asymmetric addition of open flux in the tail lobes. This open flux is produced at the beginning of the Dungey cycle [*Dungey*, 1961] when magnetic reconnection occurs between the planetary field and the IMF, creating open field lines that are circulated to the tail by the solar wind flow. As these open fields are asymmetrically added to the Earth's magnetotail, a tail twist would be observed. [*Kaymaz et al.*, 1994] utilized IMP 8 measurements to investigate the IMF control on Earth's magnetotail at ~33 Earth radii downtail and observed a nonuniform tail field distribution during periods of dominant IMF B_Y. Additionally, the results of this study revealed that the IMF B_Y cases exhibited a current sheet rotation that varied with IMF strength and downtail distance. By comparing these results with simulations of the solar wind-terrestrial magnetosphere interaction, *Kaymaz et al.* [1995] determined that the tail twist results from reconnection and related MHD motions within the magnetosphere. Many additional studies have been

conducted to investigate the magnetotail response to IMF B_Y at Earth [e.g., *Tsurutani et al.*, 1984; *Sibeck et al.*, 1985; *Macwan*, 1992].

Although Mars lacks a global intrinsic field, the dynamics at Earth indicate that attention must be paid to the occurrence of dayside reconnection and the resulting circulation of magnetic flux. Recently, MAVEN data have provided the first comprehensive example of dayside magnetic reconnection at Mars [*Harada et al., Magnetic reconnection on dayside crustal magnetic fields at Mars: MAVEN observations, submitted to Geophys. Res. Lett., 2018*]. Observations of frequent magnetic reconnection throughout the Martian magnetosphere [e.g., *Krymskii et al.*, 2002; 2004; *Halekas et al.*, 2006; 2009] suggest that the presence of intrinsic crustal magnetic fields, combined with induced magnetosphere dynamics, create a hybrid magnetosphere structure. This hybrid magnetosphere is strongly influenced by both intrinsic and induced fields, as illustrated in Figure 4.

The theory of a hybrid Martian magnetosphere, consisting of a global intrinsic dipole field contribution surrounded by induced/draped fields, was originally based on laboratory studies which identified magnetotail sectors composed of induced and intrinsic fields [*Dubinin et al.*, 1980]. Prior to the unambiguous detection of crustal magnetic fields by Mars Global Surveyor (MGS), *Slavin and Holzer* [1982] studied the Mars-solar wind interaction using Mars 2, 3, and 5 data for a comparative analysis with Venus. They concluded that a modest intrinsic magnetic dipole moment would be necessary to explain the effective bow shock shape and location. Following this work, *Axford* [1991] determined that in addition to bow shock structure, Phobos 2 measurements of tail magnetic flux content could not be attributed to induced fields alone. Conversely, *Dubinin et al.* [1994] utilized Phobos 2 electron measurements to trace magnetic field topologies in the equatorial magnetosphere and

observed a magnetotail dependence on IMF orientation, suggesting an induced magnetosphere interaction.

More recently, MGS observations of dayside magnetic fields demonstrated an asymmetry in the distribution of draped IMF [*Brain et al.*, 2006], leaving many unanswered questions about the magnetosphere structure. *Luhmann et al.* [2015b] showed that global numerical simulations of the Mars-solar wind interaction aid the interpretation of the MGS data and posed the question of whether the axial dipole moment of Mars is truly understood. In an attempt to study the effects of an intrinsic dipole moment on the solar wind interaction and magnetotail configuration at Mars, *Kallio et al.* [2008] utilized a quasi-neutral hybrid model to simulate this interaction for varying axial-aligned dipole strengths. The resulting shape and location of the tail lobes are strikingly similar to the MAVEN observations presented here when considering the model results for a dipolar intrinsic field with a surface strength of 10 nT (see *Kallio et al.* [2008] Figure 3b). When comparing the MAVEN magnetotail observations with the MHD simulations from Figure 2, along with those from *Kallio et al.* [2008], we consider that the influence of a dipolar contribution may play a role in shaping the magnetospheric structure at Mars. The *Arkani-Hamed* [2002] spherical harmonics crustal field model implemented in the MHD model does, indeed, include a low-order dipole term. Moreover, because the modeling results in Figure 2 have been averaged over all crustal field orientations the observed trends are due to the low-order terms while the impact of the high-order terms are negligible. Although outside the scope of this study, determining whether a modest dipole moment influences the structure of the Martian magnetosphere is an important topic for future work.

In this work, we have performed a data-model comparison to statistically assess the configuration of the Martian magnetotail. Further comparison with the model results presented here, along with previous studies, suggest that this twisted tail configuration may be driven by the presence of a weak dipole term. At Earth where a strong dipole field is present, dayside magnetic reconnection occurring in the presence of a dominant IMF B_Y results in a similar twisted-tail pattern. Therefore, the presence of a modest magnetic dipole and dayside reconnection at Mars could be a possible explanation for this observed magnetotail pattern.

To further understand the cause of this Martian magnetotail configuration, future work will utilize MAVEN's continually growing data set to perform in-depth studies. These future studies will investigate the dependence of the tail twist on crustal field orientation and examine how this twist changes with downtail distance. Additionally, the influence of a modest dipole contribution will be considered as we move towards better understanding the unique structure of the Martian magnetosphere.

Acknowledgements

The MAVEN project is supported by NASA through the Mars Exploration Program. MAVEN data are publicly available through the Planetary Plasma Interactions Node of the Planetary Data System (https://pds-ppi.igpp.ucla.edu/mission/MAVEN). The simulation data used in this work can be accessed at: https://umich.box.com/s/sgvp67nxg1yuyi093xa3axvgh6s3x3zo. GAD gratefully acknowledges the artistic skills of Jessica Still and the time she dedicated to create the schematics presented in Figure 4.

References

Acuna, M. H., et al. (1998), Magnetic field and plasma observations at Mars: Initial results of the Mars global surveyor mission, *Science*, *279*(5357), 1676-1680.

Acuna, M. H., et al. (1999), Global distribution of crustal magnetization discovered by the Mars Global Surveyor MAG/ER experiment, *Science*, *284*(5415), 790-793.

Arkani-Hamed, J. (2002), An improved 50-degree spherical harmonic model of the magnetic field of Mars derived from both high-altitude and low-altitude data, *J Geophys Res-Planet*, *107*(E10).

Axford, W. I. (1991), A Commentary on Our Present Understanding of the Martian Magnetosphere, *Planet Space Sci*, *39*(1-2), 167-173.

Bertucci, C., F. Duru, N. Edberg, M. Fraenz, C. Martinecz, K. Szego, and O. Vaisberg (2011), The Induced Magnetospheres of Mars, Venus, and Titan, *Space Sci Rev*, *162*(1-4), 113-171.

Brain, D. A. (2006), Mars global surveyor measurements of the martian solar wind interaction, *Space Sci Rev*, *126*(1-4), 77-112.

Brain, D. A., D. L. Mitchell, and J. S. Halekas (2006), The magnetic field draping direction at Mars from April 1999 through August 2004, *Icarus*, *182*(2), 464-473.

Brain, D. A., R. J. Lillis, D. L. Mitchell, J. S. Halekas, and R. P. Lin (2007), Electron pitch angle distributions as indicators of magnetic field topology near Mars, *J Geophys Res-Space*, *112*(A9).

Brain, D. A., A. H. Baker, J. Briggs, J. P. Eastwood, J. S. Halekas, and T. D. Phan (2010), Episodic detachment of Martian crustal magnetic fields leading to bulk atmospheric plasma escape, *Geophys Res Lett*, *37*.

Brain, D. A., et al. (2015), The spatial distribution of planetary ion fluxes near Mars observed by MAVEN, *Geophys Res Lett*, *42*(21), 9142-9148.

Connerney, J. E. P., M. H. Acuna, P. J. Wasilewski, G. Kletetschka, N. F. Ness, H. Reme, R. P. Lin, and D. L. Mitchell (2001), The global magnetic field of Mars and implications for crustal evolution, *Geophys Res Lett*, *28*(21), 4015-4018.

Connerney, J. E. P., M. H. Acuna, N. F. Ness, G. Kletetschka, D. L. Mitchell, R. P. Lin, and H. Reme (2005), Tectonic implications of Mars crustal magnetism, *P Natl Acad Sci USA*, *102*(42), 14970-14975.

Connerney, J. E. P., J. Espley, P. Lawton, S. Murphy, J. Odom, R. Oliversen, and D. Sheppard (2015), The MAVEN Magnetic Field Investigation, *Space Sci Rev*, *195*(1-4), 257-291.

Cowley, S. W. H. (1981), Magnetospheric Asymmetries Associated with the Y-Component of the Imf, *Planet Space Sci*, *29*(1), 79-96.

Crider, D. H., D. A. Brain, M. H. Acuna, D. Vignes, C. Mazelle, and C. Bertucci (2004), Mars Global Surveyor observations of solar wind magnetic field draping around Mars, *Space Sci Rev*, *111*(1-2), 203-221.

DiBraccio, G. A., et al. (2015), Magnetotail dynamics at Mars: Initial MAVEN observations, *Geophys Res Lett*, *42*(21), 8828-8837.

DiBraccio, G. A., et al. (2017), MAVEN observations of tail current sheet flapping at Mars, *J Geophys Res-Space*, *122*(4), 4308-4324.

Dong, C. F., S. W. Bougher, Y. J. Ma, G. Toth, Y. N. Lee, A. F. Nagy, V. Tenishev, D. J. Pawlowski, M. R. Combi, and D. Najib (2015), Solar wind interaction with the Martian upper atmosphere: Crustal field orientation, solar cycle, and seasonal variations, *J Geophys Res-Space*, *120*(9), 7857-7872.

Dong, Y., X. Fang, D. A. Brain, J. P. McFadden, J. S. Halekas, J. E. Connerney, S. M. Curry, Y. Harada, J. G. Luhmann, and B. M. Jakosky (2015), Strong plume fluxes at Mars observed

by MAVEN: An important planetary ion escape channel, *Geophys Res Lett*, *42*(21), 8942-8950.
Dong, Y., X. Fang, D. A. Brain, J. P. McFadden, J. S. Halekas, J. E. P. Connerney, F. Eparvier, L. Andersson, D. Mitchell, and B. M. Jakosky (2017), Seasonal variability of Martian ion escape through the plume and tail from MAVEN observations, *J Geophys Res-Space*, *122*(4), 4009-4022.
Dubinin, E., R. Lundin, O. Norberg, and N. Pissarenko (1993), Ion-Acceleration in the Martian Tail - Phobos Observations, *J Geophys Res-Space*, *98*(A3), 3991-3997.
Dubinin, E., R. Lundin, and K. Schwingenschuh (1994), Solar-Wind Electrons as Tracers of the Martian Magnetotail Topology, *J Geophys Res-Space*, *99*(A11), 21233-21240.
Dubinin, E., et al. (2008), Structure and dynamics of the solar wind/ionosphere interface on Mars: MEX-ASPERA-3 and MEX-MARSIS observations, *Geophys Res Lett*, *35*(11).
Dubinin, E., M. Fraenz, A. Fedorov, R. Lundin, N. Edberg, F. Duru, and O. Vaisberg (2011), Ion Energization and Escape on Mars and Venus, *Space Sci Rev*, *162*(1-4), 173-211.
Dubinin, E., et al. (2017), The Effect of Solar Wind Variations on the Escape of Oxygen Ions From Mars Through Different Channels: MAVEN Observations, *J Geophys Res-Space*, *122*(11), 11285-11301.
Dubinin, E. M., P. L. Izraelevich, and I. M. Podgorny (1980), The combined magnetosphere, *Kosmicheskie Issledovaniia*, *18*, 470-474.
Dungey, J. W. (1961), Steady State of Chapman-Ferraro Problem in 2 Dimensions, *J Geophys Res*, *66*(4), 1043-&.
Eastwood, J. P., D. A. Brain, J. S. Halekas, J. F. Drake, T. D. Phan, M. Oieroset, D. L. Mitchell, R. P. Lin, and M. Acuna (2008), Evidence for collisionless magnetic reconnection at Mars, *Geophys Res Lett*, *35*(2).
Eastwood, J. P., J. J. H. Videira, D. A. Brain, and J. S. Halekas (2012), A chain of magnetic flux ropes in the magnetotail of Mars, *Geophys Res Lett*, *39*.
Fedorov, A., et al. (2006), Structure of the martian wake, *Icarus*, *182*(2), 329-336.
Halekas, J. S., D. A. Brain, R. J. Lillis, M. O. Fillingim, D. L. Mitchell, and R. P. Lin (2006), Current sheets at low altitudes in the Martian magnetotail, *Geophys Res Lett*, *33*(13).
Halekas, J. S., J. P. Eastwood, D. A. Brain, T. D. Phan, M. Oieroset, and R. P. Lin (2009), In situ observations of reconnection Hall magnetic fields at Mars: Evidence for ion diffusion region encounters, *J Geophys Res-Space*, *114*.
Halekas, J. S., E. R. Taylor, G. Dalton, G. Johnson, D. W. Curtis, J. P. McFadden, D. L. Mitchell, R. P. Lin, and B. M. Jakosky (2015), The Solar Wind Ion Analyzer for MAVEN, *Space Sci Rev*, *195*(1-4), 125-151.
Halekas, J. S., et al. (2016), Plasma clouds and snowplows: Bulk plasma escape from Mars observed by MAVEN, *Geophys Res Lett*, *43*(4), 1426-1434.
Halekas, J. S., et al. (2017), Structure, dynamics, and seasonal variability of the Mars-solar wind interaction: MAVEN Solar Wind Ion Analyzer in-flight performance and science results, *J Geophys Res-Space*, *122*(1), 547-578.
Hara, T., et al. (2017), On the origins of magnetic flux ropes in near-Mars magnetotail current sheets, *Geophys Res Lett*, *44*(15), 7653-7662.
Harada, Y., et al. (2015a), Magnetic reconnection in the near-Mars magnetotail: MAVEN observations, *Geophys Res Lett*, *42*(21), 8838-8845.
Harada, Y., et al. (2015b), Marsward and tailward ions in the near-Mars magnetotail: MAVEN observations, *Geophys Res Lett*, *42*(21), 8925-8932.
Harada, Y., et al. (2017), Survey of magnetic reconnection signatures in the Martian magnetotail with MAVEN, *J Geophys Res-Space*, *122*(5), 5114-5131.
Harada et al., Magnetic reconnection on dayside crustal magnetic fields at Mars: MAVEN observations, submitted to Geophys. Res. Lett., 2018

Jakosky, B. M., et al. (2015), The Mars Atmosphere and Volatile Evolution (MAVEN) Mission, *Space Sci Rev*, *195*(1-4), 3-48.
Kallio, E., S. Barabash, P. Janhunen, and R. Jarvinen (2008), Magnetized Mars: Transformation of Earth-like magnetosphere to Venus-like induced magnetosphere, *Planet Space Sci*, *56*(6), 823-827.
Kaymaz, Z., G. L. Siscoe, J. G. Luhmann, R. P. Lepping, and C. T. Russell (1994), Interplanetary Magnetic-Field Control of Magnetotail Magnetic-Field Geometry - Imp-8 Observations, *J Geophys Res-Space*, *99*(A6), 11113-11126.
Kaymaz, Z., G. Siscoe, J. G. Luhmann, J. A. Fedder, and J. G. Lyon (1995), Interplanetary Magnetic-Field Control of Magnetotail Field - Imp-8 Data and Mhd Model Compared, *J Geophys Res-Space*, *100*(A9), 17163-17172.
Krymskii, A. M., T. K. Breus, N. F. Ness, M. H. Acuna, J. E. P. Connerney, D. H. Crider, D. L. Mitchell, and S. J. Bauer (2002), Structure of the magnetic field fluxes connected with crustal magnetization and topside ionosphere at Mars, *J Geophys Res-Space*, *107*(A9).
Krymskii, A. M., N. F. Ness, D. H. Crider, T. K. Breus, M. H. Acuna, and D. P. Hinson (2004), Solar wind interaction with the ionosphere/atmosphere and crustal magnetic fields at Mars: Mars Global Surveyor Magnetometer/Electron Reflectometer, radio science, and accelerometer data, *J Geophys Res-Space*, *109*(A11).
Liemohn, M. W., S. S. Xu, C. F. Dong, S. W. Bougher, B. C. Johnson, R. Ilie, and D. L. De Zeeuw (2017), Ionospheric control of the dawn-dusk asymmetry of the Mars magnetotail current sheet, *J Geophys Res-Space*, *122*(6), 6397-6414.
Luhmann, J. G., C. T. Russell, K. Schwingenschuh, and Y. Yeroshenko (1991), A Comparison of Induced Magnetotails of Planetary Bodies - Venus, Mars, and Titan, *J Geophys Res-Space*, *96*(A7), 11199-11208.
Luhmann, J. G., et al. (2015a), Implications of MAVEN Mars near-wake measurements and models, *Geophys Res Lett*, *42*(21), 9087-9094.
Luhmann, J. G., Y. J. Ma, D. A. Brain, D. Ulusen, R. J. Lillis, J. S. Halekas, and J. R. Espley (2015b), Solar wind interaction effects on the magnetic fields around Mars: Consequences for interplanetary and crustal field measurements, *Planet Space Sci*, *117*, 15-23.
Lundin, R. (2011), Ion Acceleration and Outflow from Mars and Venus: An Overview, *Space Sci Rev*, *162*(1-4), 309-334.
Ma, Y. J., A. F. Nagy, I. V. Sokolov, and K. C. Hansen (2004), Three-dimensional, multispecies, high spatial resolution MHD studies of the solar wind interaction with Mars, *J Geophys Res-Space*, *109*(A7).
Macwan, S. E. (1992), A Determination of Twisting of the Earths Magnetotail at Distances 115-220 Re - Isee 3, *J Geophys Res-Space*, *97*(A12), 19239-19249.
Nagy, A. F., et al. (2004), The plasma environment of Mars, *Space Sci Rev*, *111*(1-2), 33-114.
Romanelli, N., C. Bertucci, D. Gomez, and C. Mazelle (2015), Dependence of the location of the Martian magnetic lobes on the interplanetary magnetic field direction: Observations from Mars Global Surveyor, *J Geophys Res-Space*, *120*(9), 7737-7747.
Sibeck, D. G., G. L. Siscoe, J. A. Slavin, E. J. Smith, B. T. Tsurutani, and R. P. Lepping (1985), The Distant Magnetotails Response to a Strong Interplanetary Magnetic-Field by - Twisting, Flattening, and Field Line Bending, *J Geophys Res-Space*, *90*(Na5), 4011-4019.
Slavin, J. A., and R. E. Holzer (1982), The Solar-Wind Interaction with Mars Revisited, *J Geophys Res*, *87*(Nb12), 285-296.
Tsurutani, B. T., D. E. Jones, R. P. Lepping, E. J. Smith, and D. G. Sibeck (1984), The Relationship between the Imf by and the Distant Tail (150-238 Re) Lobe and Plasmasheet by Fields, *Geophys Res Lett*, *11*(10), 1082-1085.

Weber, T., D. A. Brain, D. L. Mitchell, S. Xu, J. E. P. Connerney, and J. S. Halekas (2017), Characterization of Low-Altitude Nightside Martian Magnetic Topology Using Electron Pitch Angle Distributions, *Journal of Geophysical Research- Space Physics*, *122*(10).
Xu, S. S., et al. (2017a), Martian low-altitude magnetic topology deduced from MAVEN/SWEA observations, *J Geophys Res-Space*, *122*(2), 1831-1852.
Xu, S. S., et al. (2017b), High-Altitude Closed Magnetic Loops at Mars Observed by MAVEN, *Geophys Res Lett*, *44*(22), 11229-11238.
Yeroshenko, Y., W. Riedler, K. Schwingenschuh, J. G. Luhmann, M. Ong, and C. T. Russell (1990), The Magnetotail of Mars - Phobos Observations, *Geophys Res Lett*, *17*(6), 885-888.

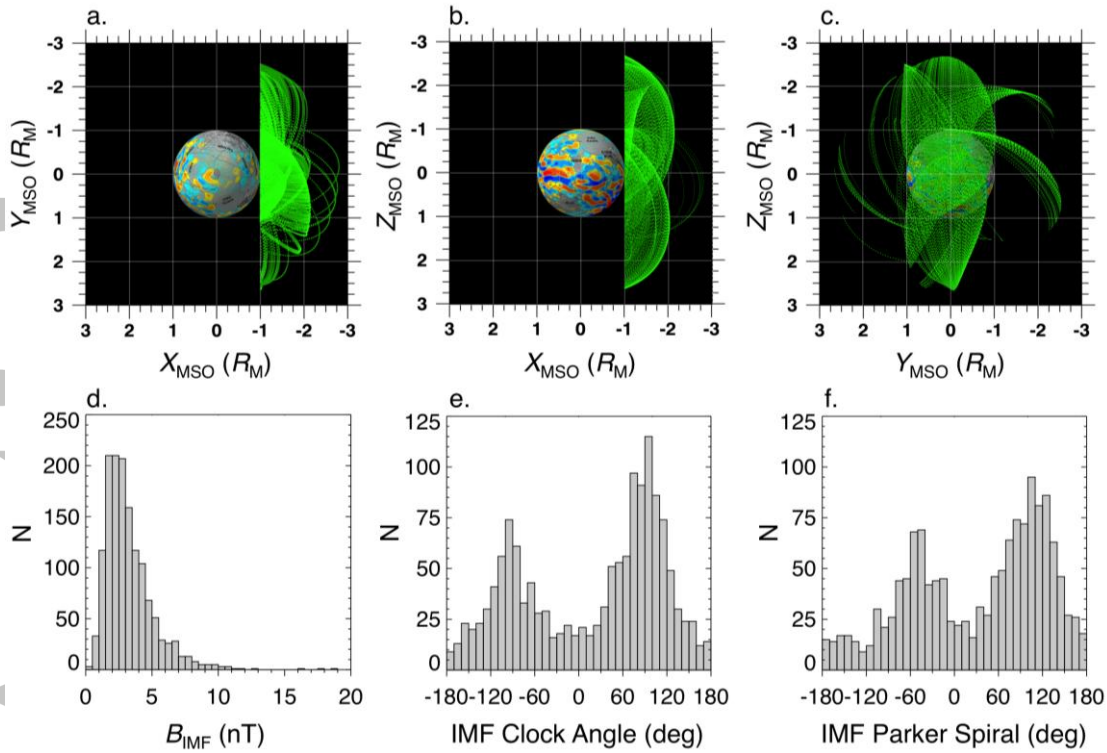

Figure 1. a-c) MAVEN orbital trajectories in the Martian magnetotail ($X_{MSO} \leq -1\ R_M$) included in this study. Views are shown a) in the equatorial plane, b) in the meridional plane, and c) from the tail towards Mars. An arbitrary crustal field orientation is depicted *Connerney et al.* [2005]. d-f) Distributions of measured quantities are displayed for d) IMF magnitude, e) IMF clock angle, and f) IMF Parker spiral angle.

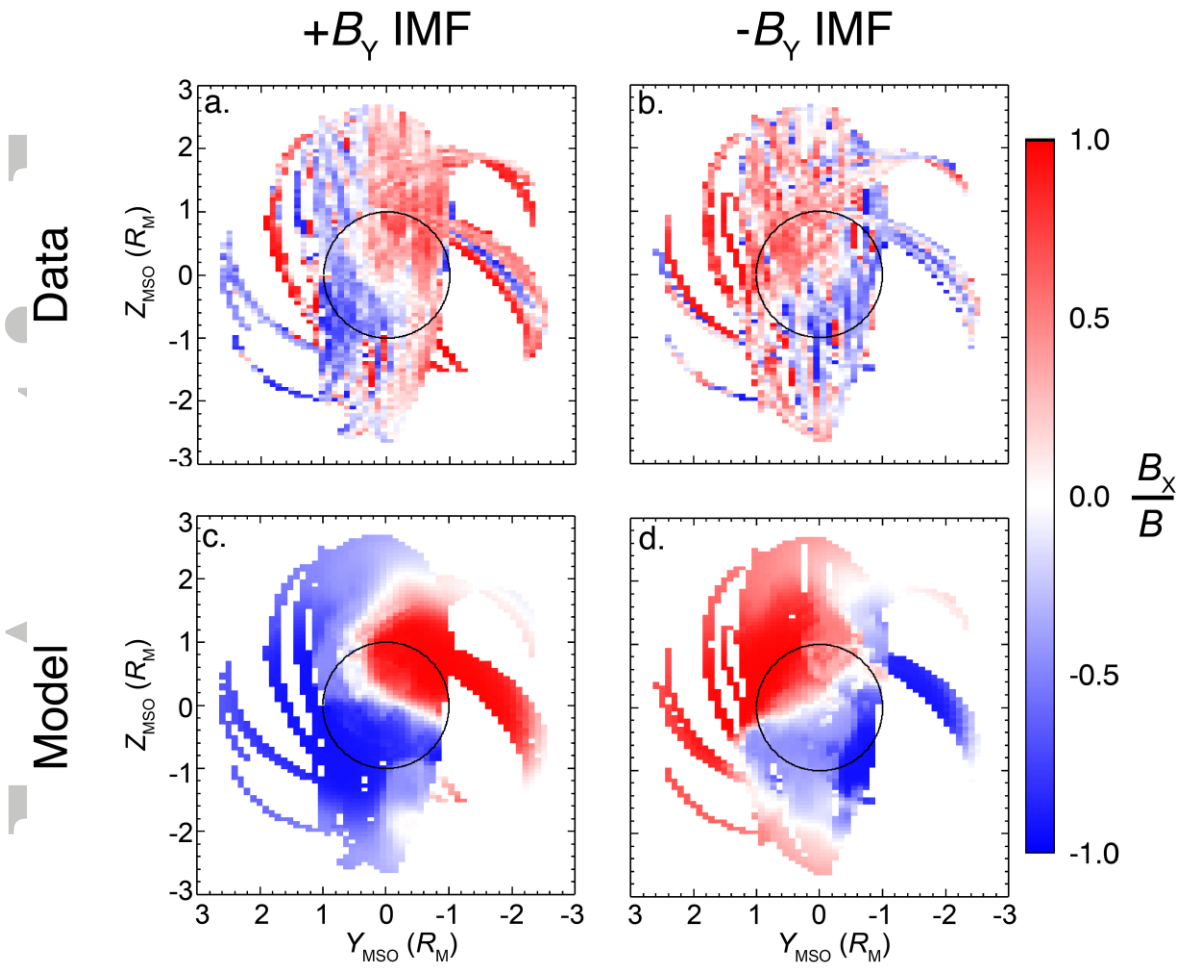

Figure 2. Cross-tail projections of the normalized B_X component in the Martian magnetotail as viewed from the tail towards Mars. Changes in tail configuration based on IMF periods of $\pm B_Y$ (as indicated by columns) are shown for a-b) MAVEN observations and c-d) MHD simulations. Red and blue colors represent the sunward ($+B_X/B$, into the page) and anti-sunward ($-B_X/B$, out of the page) directions, respectively.

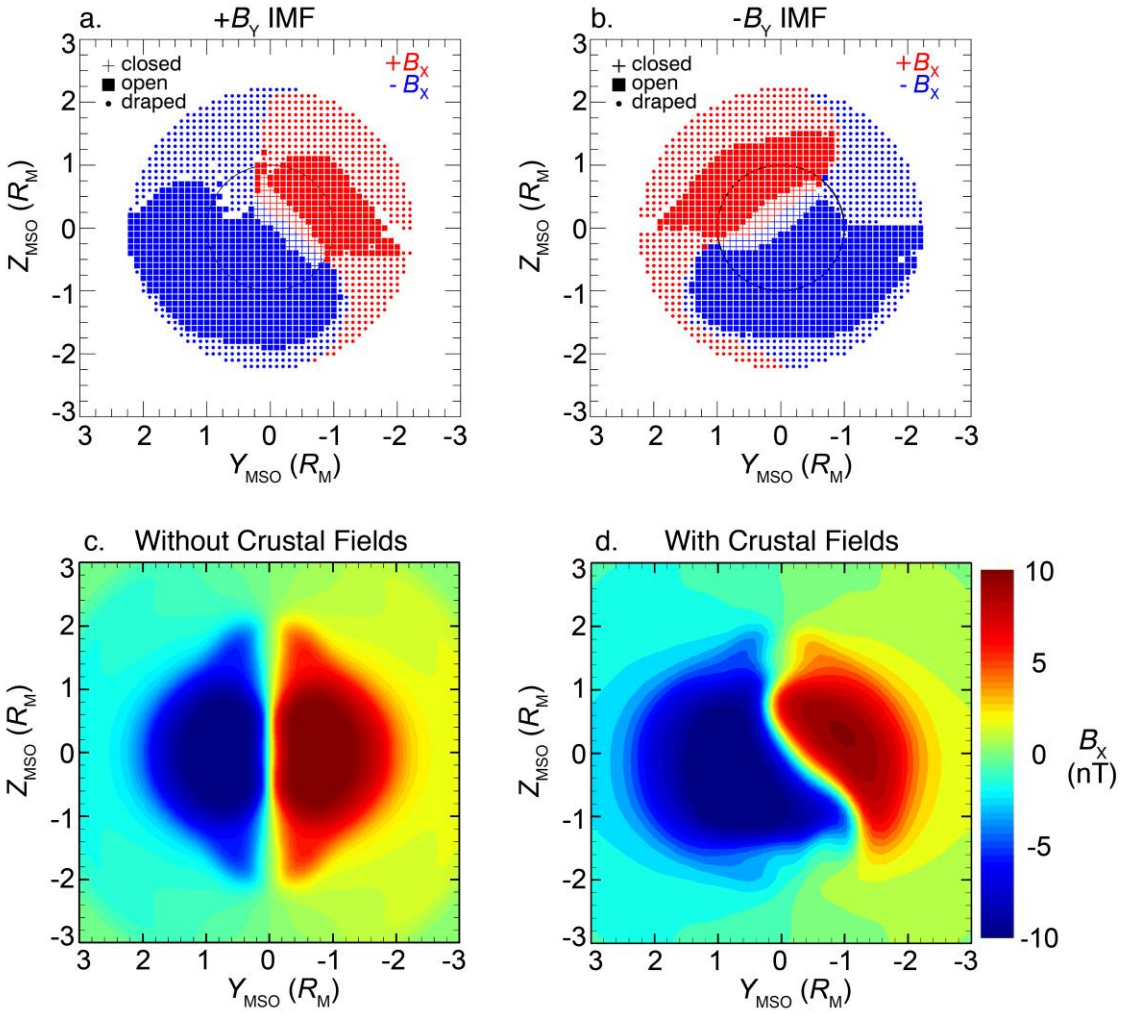

Figure 3. Simulation results are presented using cross-tail slices at 2 R_M downtail. a-b) Magnetic field topologies determined by field line tracings performed on MHD simulations, are shown for IMF periods of a) +B_Y and b) -B_Y. As viewed from the tail towards Mars, red and blue colors represent the sunward (+B_X/B) and anti-sunward (-B_X/B) directions, respectively. Symbols represent closed (+), open (■), and draped (•) field topologies. c-d) Tail configurations are compared for the +B_Y IMF case both c) without and d) with the *Arkani-Hamed* [2002] crustal field model.

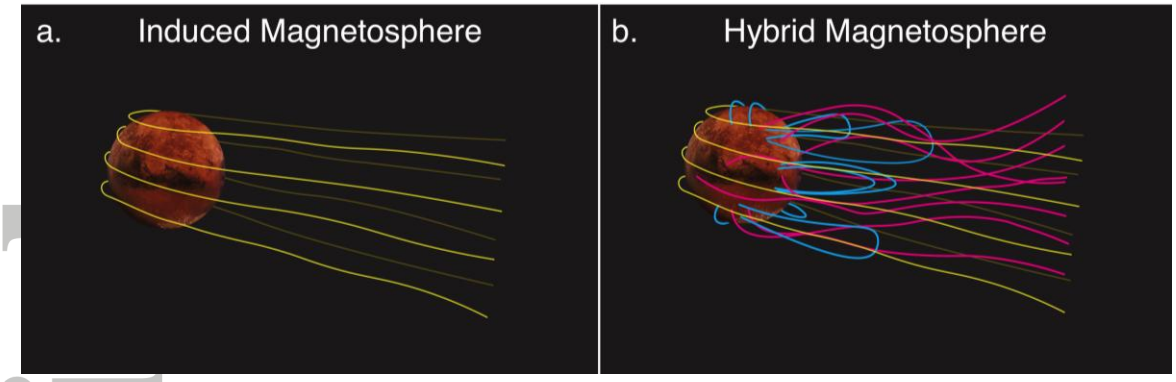

Figure 4. Schematics of a) an induced Martian magnetosphere similar to a Venus- or comet-like interaction with draped IMF magnetic fields (yellow) and b) a hybrid Martian magnetosphere including open (magenta), closed (cyan), and draped (yellow) field topologies.